Chinese Chemical Letters 33 (2022) 385–389

Contents lists available at ScienceDirect

Chinese Chemical Letters

journal homepage: www.elsevier.com/locate/cclet

Nitrogen-doped Co_3O_4 nanowires enable high-efficiency electrochemical oxidation of 5-hydroxymethylfurfural

Mengxiao Sun[a], Yue Wang[a], Chunsen Sun[a], Yan Qi[a,*], Jia Cheng[a], Yumei Song[b,*], Lixue Zhang[a,*]

[a] College of Chemistry and Chemical Engineering, State Key Laboratory of Bio-fibers and Eco-textiles, Qingdao University, Qingdao 266071, China
[b] Guangdong Provincial Key Laboratory of Emergency Test for Dangerous Chemicals, Institute of Analysis, Guangdong Academy of Sciences, Guangzhou 510070, China

ARTICLE INFO

Article history:
Received 31 March 2021
Revised 29 April 2021
Accepted 7 May 2021
Available online 19 May 2021

Keywords:
Electrochemical oxidation
HMF
FDCA
Co_3O_4
Nitrogen doping

ABSTRACT

Developing highly efficient and cost-effective catalysts for electrochemically oxidizing biomass-derived 5-hydroxymethylfurfural (HMF) into value-added 2,5-furandicarboxylic acid (FDCA) is of great importance. Herein, we report a controllable nitrogen doping strategy to significantly improve the catalytic activity of Co_3O_4 nanowires for highly selective electro-oxidation of HMF into FDCA. The nitrogen doping leads to the generation of defects including nitrogen dopants and oxygen vacancies in Co_3O_4 nanowires, which is conducive to the formation of catalytically active sites. As a result, the electro-oxidation potential for HMF is only 1.38 V (*vs.* RHE) when the current density reaches 50 mA/cm^2. More importantly, the conversion rate of HMF is as high as 99.5%, and the yield of FDCA is up to 96.4%.

Biomass is a kind of abundant carbon neutral renewable resource, which can be used to produce bio-energy and biological materials [1,2]. Thus, substitution of petroleum-based chemicals with biomass and its derivatives will play a key role in sustaining the growth of the chemical industry since the large-scale consumption of fossil fuel leads to global energy shortages and climate deterioration [3]. As a biomass derivative, 5-hydroxymethylfurfural (HMF) is an important platform chemical, since HMF can be further converted into high-value-added versatile chemicals [4,5]. In particular, 2,5-furandicarboxylic acid (FDCA), which can be obtained by the selective oxidation of HMF, is an important monomer to produce polymeric materials [6–8]. However, the kinetics of selective oxidation of alcohol groups of HMF to carboxylic acids is slow, thus the oxidation reaction of HMF usually occurs under high temperature and pressure to speed up the conversion [9,10].

In recent years, electrochemical catalysis becomes a favorable approach for the selective conversion of organic compounds, which is completely driven by electrochemical potential and does not require harsh oxidation conditions. Since the electrocatalytic synthesis of FDCA from HMF was firstly reported by Grabowski and colleagues in 1991 [11], the selective electrochemical oxidation of HMF to FDCA has attracted considerable attentions. Interestingly, the HMF oxidation reaction can be regarded as a substitute for the oxygen evolution reaction (OER) on the anode in the water electrolysis process. While realizing the production of high value-added FDCA, it also realizes the production of green hydrogen at low voltage. To reduce the overpotential during HMF oxidation, developing high-performance electro-catalysts for HMF oxidation is highly desired. Li and colleagues demonstrated the selective from HMF to FDCA on a bimetallic Pd-Au catalyst [12]. Kim and colleagues investigated the catalytic performance of Pd and Au toward the selective oxidation of ethanol and aldehyde of HMF [13]. To replace the noble metal catalysts, transition metal-based electrocatalysts for HMF oxidation have been explored [14–22]. Sun and colleagues reported the coupling of HMF oxidation and H_2 evolution in alkaline medium by using a variety of low-cost cobalt-nickel composites such as Ni_2P, Co-P and Ni_3S_2 [23–25]. Recently, spinel Co_3O_4 has been developed as non-noble metal electrocatalyst for HMF oxidation. For instance, Zhang and colleagues reported that Co_3O_4 nanowires *in situ* grown on nickel foam showed a reasonable performance for electro-oxidation of HMF [26]. Compared with the well-reported environmental materials such as MnO_2 [27,28], Co_3O_4 possesses a more variable Co valence and well-established fabrication strategies [29], and thus may hold a more promising potential application in HMF electrocatalysis.

* Corresponding authors.
E-mail addresses: qddxqy@qdu.edu.cn (Y. Qi), symei2011@163.com (Y. Song), zhanglx@qdu.edu.cn (L. Zhang).

https://doi.org/10.1016/j.cclet.2021.05.009
1001-8417/

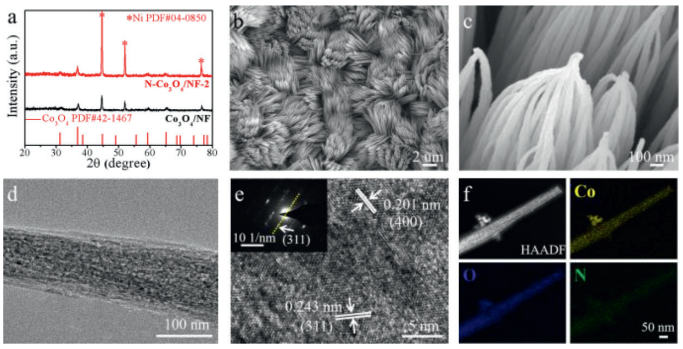

Fig. 1. (a) XRD pattern of Co_3O_4/NF and N-Co_3O_4/NF-2 with the corresponding standard patterns of Co_3O_4 and Ni. (b, c) SEM images of N-Co_3O_4/NF-2 at different magnifications. (d) TEM and (e) HRTEM images of N-Co_3O_4, the inset of Fig. 1e is SAED pattern of N-Co_3O_4. (f) EDS elemental mapping images of N-Co_3O_4.

Although composition and nanostructure control are widely used to develop electrocatalysts for HMF oxidation, to enhance the HMF oxidation performance of electrocatalysts *via* electronic structure modulation through defect engineering strategy is rarely reported. Herein, we report a nitrogen-doping strategy to enhance the HMF electro-oxidation performance of Co_3O_4 nanoarray electrocatalyst. It is found that after low-temperature ammonia treatment of Co_3O_4 nanowire arrays on nickel foam (Co_3O_4/NF), nitrogen-doped Co_3O_4/NF (N-Co_3O_4/NF) can be easily obtained. Compared with pristine Co_3O_4/NF, N-Co_3O_4/NF samples exhibit lower HMF oxidation overpotentials. When the current density reaches 50 mA/cm^2, the electro-oxidation potential of HMF is only 1.38 V (*vs*. RHE). The conversion rate of HMF is up to 99.5%, and the yield of FDCA is stable at around 96.4%. These results indicate that nitrogen doping can effectively improve the HMF electro-oxidation performance of Co_3O_4, which should be attributed to the effective regulation of the electronic structure of Co_3O_4 by nitrogen doping and the formed oxygen vacancies.

The N-Co_3O_4/NF catalysts were fabricated by a facile process as illustrated in Scheme S1 (Supporting information). The Co_3O_4 nanowire arrays were firstly grown onto NF by a simple hydrothermal reaction and a subsequent pyrolysis [30]. Then, Co_3O_4/NF was converted into N-Co_3O_4/NF at certain temperatures under NH_3 atmosphere, and the N-Co_3O_4/NF samples obtained at 150, 250, 350 and 450 °C were denoted as N-Co_3O_4/NF-1, N-Co_3O_4/NF-2, N-Co_3O_4/NF-3 and N-Co_3O_4/NF-4, respectively. The X-ray diffraction (XRD) patterns of N-Co_3O_4/NF-2 present diffraction peaks at 31.2°, 36.8°, 59.3° and 65.2° (Fig. 1a), which can be assigned to the (220), (311), (511) and (440) lattice planes of Co_3O_4 (JCPDS No. 42-1467), respectively. This result indicates that nitrogen doped Co_3O_4 largely maintains the crystalline structure of Co_3O_4 after ammonia treatment at 250 °C. Interestingly, the diffraction peaks of N-Co_3O_4 samples shift negatively with increasing the nitridation temperature, and no obvious phase change can be observed until the temperature reached 350 °C (Fig. S1 in Supporting information), indicating a partial substitution of O atoms by N atoms during the low temperature nitrogen doping process [31]. For N-Co_3O_4/NF-3, the occurrence of impurity phase is distinct, and the peaks located at 36.4°, 42.3° and 61.4° belong to the (111), (200) and (220) planes of CoO (JCPDS No. 48-1719), implying that part of Co_3O_4 was reduced to CoO by ammonia. Moreover, the diffraction peaks of Co_3O_4 crystal disappears when the nitridation temperature reached 450 °C, conjecturing that Co_3O_4 is reduced to metallic Co. Note that there are no clear diffraction peaks for metallic Co can be distinguished due to the interference by strong Ni signals (Fig. S1) [32]. However, the high-resolution transmission electron microscopy (HRTEM) image and selected area electron diffraction (SAED) results verify the formation of metallic Co in the N-Co_3O_4/NF-4 products (Fig. S2 in Supporting information).

Scanning electron microscopy (SEM) images present that the prepared N-Co_3O_4 nanowires grow vertically and uniformly on NF surface (Figs. 1b and c), which maintains the initial morphology of Co_3O_4 nanowire array structure (Fig. S3 in Supporting information). As shown in Fig. S4 (Supporting information), a side-view SEM image displays that the NiO-Co_3O_4 nanoneedle array is uniformly aligned on the Ni foam substrate and the thickness of these nanoneedle is around 3–4 μm. With increasing the temperature of ammonia treatment, the Co_3O_4 nanowire structure gradually collapsed (Fig. S5 in Supporting information). TEM image of N-Co_3O_4/NF-2 is shown in Fig. 1d, which further evident that N-Co_3O_4 is composed of nanoparticles aligned to form nanowire structure. HRTEM image presents two sets of lattices spacing with distances of 0.201 nm and 0.243 nm (Fig. 1e), belonging to the (400) and (311) facets of Co_3O_4, respectively. The inset image of Fig. 1e is the SAED pattern of N-Co_3O_4, which also confirms the polycrystalline structure and shows the (311) crystal faces of Co_3O_4. Furthermore, the energy dispersive spectrometer (EDS) elemental mapping images show that Co, O and N elements are uniformly distributed in the nanowire (Fig. 1f), confirming the successful doping of N element.

To further investigate the effect of nitrogen doping into Co_3O_4, X-ray photoelectron spectroscopy (XPS) tests were performed (Fig. 2). The survey spectra confirm the existence of Co, N and O elements in N-Co_3O_4/NF-2 (Fig. 2a). The peak at approximately 397.8 eV corresponds to Co-N bond formed between Co and N [31,33], which further confirm the successful doping of N element (Fig. 2b). The peaks at 406.7 eV and 399.2 eV in N 1s region are assigned to NO_3^- species and the surface chemisorbed N_2, respectively. In the Co 2p region, the peaks at 794.5 and 779.4 eV belong to the Co^{3+} species of N-Co_3O_4/NF-2, and the peaks at 796.4 and 781.1 eV and the two satellites peaks at 803 and 787 eV correspond to the Co^{2+} species of N-Co_3O_4/NF-2 (Fig. 2c) [33,34]. It is found that the mole ratio of Co^{2+}/Co^{3+} in N-Co_3O_4 becomes larger than that of pristine Co_3O_4, which agrees well with the previous report [31]. Besides, the Co 2p peaks of N-Co_3O_4/NF shift negatively with increasing the nitridation temperature (Fig. S6 in Supporting information). It is deduced that the partial replacement of lattice O by N leads to the increase of electron density around the Co species [31]. In Fig. 2d, the O 1s spectrum can be fitted to three different oxygen species: O1 (529.6 eV), O2 (531.4 eV) and O3 (532.5 eV) are assigned to the lattice oxygen in Co−O, surface chemisorbed oxygen, and unavoidable surface water molecules, respectively [35]. As observed, the relative intensity of O1 decreases and the intensity of O2 is significantly enhanced after the nitrogen doping, indicating that the N dopants can lead to the formation of surface oxygen vacancies. The formation of oxygen vacancies will induce the reduction of Co valence state (lower Co^{3+}/Co^{2+} ratio in Co_3O_4), which can intermediate the easier construction of CoOOH active sites when applying a positive potential [36,37]. With increasing the ammonia treatment temperature, the O2/O1 ratio increases gradually (Fig. S7 in Supporting information), and noticeably the signal strength of the Co-N bond also gradually increased (Fig. S8 in Supporting information), indicating that more N atoms are successfully doped into the lattice of Co_3O_4.

As reported, OER competes with the electrocatalytic oxidation of HMF to FDCA under alkaline condition. OER and HMF oxidation electrocatalytic capability of the prepared N-Co_3O_4/NF samples was evaluated in 1.0 mol/L KOH solution. As shown in Fig. 3a, the linear sweep voltammetry (LSV) curve of N-Co_3O_4/NF-2 in 1.0 mol/L KOH solution shows an onset potential of about 1.51 V *vs*. RHE to drive OER. Meanwhile, after adding 50 mmol/L HMF into 1.0 mol/L KOH solution, N-Co_3O_4/NF-2 only requires an onset potential of about 1.26 V *vs*. RHE to drive an oxidation reaction, which implies

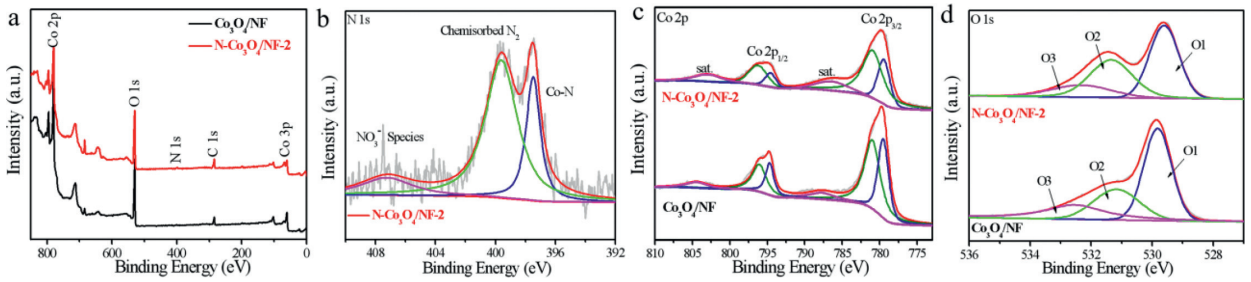

Fig. 2. (a) XPS survey spectra of Co_3O_4/NF and N-Co_3O_4/NF-2. XPS spectra of (b) N 1s and (c) Co 2p regions. XPS spectra of Co_3O_4/NF and N-Co_3O_4/NF-2 in the (d) O 1s region.

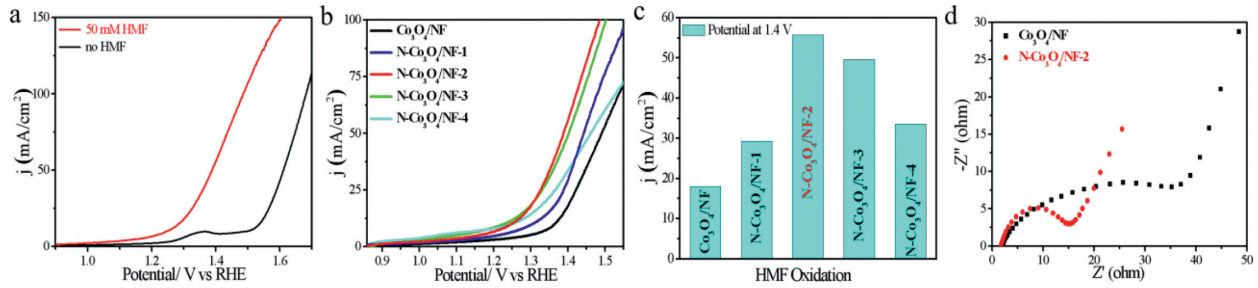

Fig. 3. (a) LSV curves of N-Co_3O_4/NF-2 in 1.0 mol/L KOH with or without 50 mmol/L HMF. (b) LSV curves of Co_3O_4/NF and N-Co_3O_4/NF samples in 1.0 mol/L KOH with 50 mmol/L HMF. (c) Current density of Co_3O_4/NF and N-Co_3O_4/NF samples 1.4 V *vs*. RHE in 1.0 mol/L KOH with 50 mmol/L HMF. (d) Nyquist plots of Co_3O_4/NF and N-Co_3O_4/NF-2 in 1.0 mol/L KOH.

that N-Co_3O_4/NF-2 is able to preferably catalyze the oxidation of HMF at lower potentials. As shown in Fig. S9 (Supporting information), the onset potential of NF toward HMF oxidation is about 1.53 V, which is about 270 mV higher than that of N-Co_3O_4/NF-2. This phenomenon shows that the high catalytic performance of N-Co_3O_4/NF-2 on oxidizing HMF mainly comes from N-Co_3O_4. All the N-Co_3O_4/NF samples show better HMF oxidation catalytic activities than pristine Co_3O_4 (Fig. 3b), revealing that nitrogen doping effectively improves the HMF oxidation performance of Co_3O_4. Furthermore, compared with other N-Co_3O_4/NF samples, it is evident that N-Co_3O_4/NF-2 possesses the lowest onset potential and the most significant current signal toward the oxidation of HMF (Figs. 3b and c). When the anodic potential is set at 1.4 V *vs*. RHE, the current density for N-Co_3O_4/NF-2 is 55 mA/cm^2, which is obviously larger than Co_3O_4/NF (18 mA/cm^2) and other N-Co_3O_4/NF samples.

It has been demonstrated that the doping of nitrogen into the lattice of Co_3O_4 can lead to the formation of many surface oxygen vacancies and the optimization of the electronic structure of Co [33]. Especially, the existence of oxygen vacancy will intermediate the easier reconstruction of Co-OOH active sites in N-Co_3O_4/NF and improve the electrical conductivity of Co_3O_4 [36], which effectively accelerates the HMF oxidation. Moreover, electrochemical impedance spectroscopy (EIS) data show that N-Co_3O_4/NF-2 electrode possesses a much smaller charge transfer resistance (17 Ω) than that of Co_3O_4/NF (50 Ω) (Fig. 3d), indicating that the nitrogen doping endows Co_3O_4 with a more desirable electron transfer kinetics. In addition, the double-layer capacitance (C_{dl}) was calculated. As shown in Figs. S10a–f (Supporting information), the C_{dl} value of N-Co_3O_4/NF-2 is 73.7 mF/cm^2, which is larger than those of Co_3O_4/NF (12.9 mF/cm^2), N-Co_3O_4/NF-1 (14.3 mF/cm^2), N-Co_3O_4/NF-3 (17.1 mF/cm^2) andN-Co_3O_4/NF-3 (61.4 mF/cm^2), indicating that N-Co_3O_4/NF-2 also has much more active sites than other samples. The above-mentioned changes brought about by N doping to Co_3O_4 realize the improvement of its electro-catalytic performance toward HMF oxidation.

As shown in Fig. 4a, the oxidation of HMF firstly forms 5-hydroxymethyl-2-furancarboxylic acid (HMFCA) or 2,5-diformylfuran (DFF). Subsequently, HMFCA and DFF are oxidized consecutively to convert to 5-formyl-2-furancarboxylic acid (FFCA) and finally to FDCA [8,38–40]. To qualitatively and quantitatively investigate the catalytic performance of N-Co_3O_4/NF-2 toward the oxidation of HMF, a 5 h electrolysis of HMF oxidation was performed with a N-Co_3O_4/NF-2 electrode in 1.0 mol/L KOH containing 10 mmol/L HMF at 1.423 V *vs*. RHE, and the products were then tested by high performance liquid chromatography (HPLC). Fig. S11 (Supporting information) show the standard curves of HMF and FDCA obtained on the basis of the relationship between retention time and response peak area with an ultraviolet detector. To monitor the HMF oxidation process, the electrolyte samples were collected periodically and then analyzed by HPLC [38,39]. With increasing the electrolysis time, the concentration of HMF decreased obviously, and the concentration of FDCA increased significantly (Fig. S12 in Supporting information). The electrolyte containing HMF changes from yellow to colorless after potentiostatic electrolysis (Fig. S13 in Supporting information), indicating the conversion of HMF. Fig. 4b shows the curve between HMF and product concentration changes with the increasing amount of charge. At the end of electrolysis, a HMF conversion rate of 99.5%, a FDCA yield of 96.4% and a Faradaic efficiency of 97.3% are obtained with the aid of N-Co_3O_4/NF-2, and the electro-catalytic performance is very comparable with the recently reported electro-catalysts (Table S1 in Supporting information), suggesting that N-Co_3O_4/NF-2 is a highly active and selective electro-catalyst for the oxidation of HMF to FDCA. It is worth mentioning that HMFCA appeared as the major intermediate and DFF was almost not detected during the total reaction period, indicating the more favorable oxidation of the aldehyde group of HMF in our system. To assess the electrochemical durability of N-Co_3O_4/NF-2, four successive HMF electrolysis cycles were conducted at 1.423 V *vs*. RHE, and the HMF conversion rate, FDCA yield and Faradaic efficiency remains almost unchanged, indicating an excellent durability (Fig. 4c).

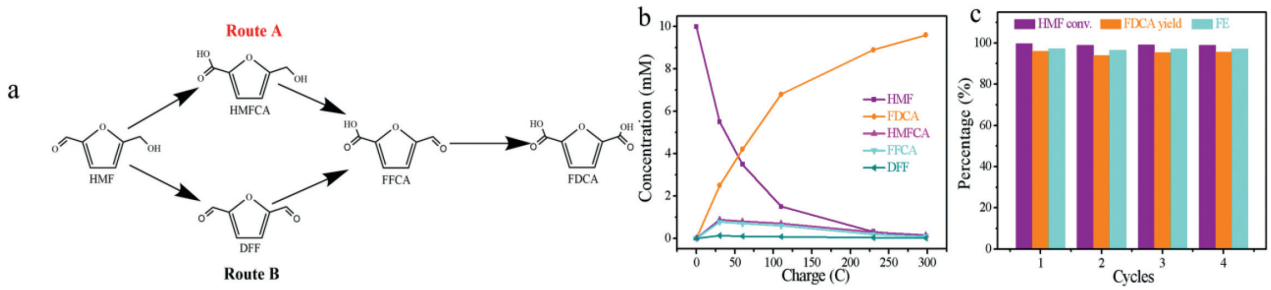

Fig. 4. (a) Two possible pathways for HMF oxidation to FDCA. (b) Conversion rate and products yield of HMF oxidation with a N-Co_3O_4/NF-2 electrode in 1.0 mol/L KOH containing 10 mmol/L HMF at an applied potential of 1.423 V *vs.* RHE. (c) HMF conversion rate, FDCA yield and Faradaic efficiency (FE) for four cyclic tests.

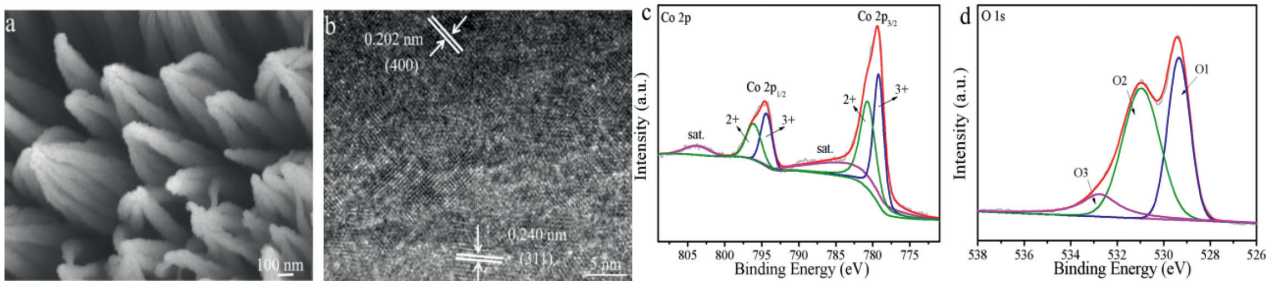

Fig. 5. (a) SEM and (b) HRTEM images of N-Co_3O_4/NF-2 after four successive HMF electrolysis. XPS spectra of N-Co_3O_4/NF-2 in the (c) Co 2p and (d) O 1s regions.

The structural stability is also an important issue for electrocatalysts. SEM, TEM and HRTEM results conclude that N-Co_3O_4/NF-2 still preserves its nanowire array morphology and crystalline structure after the anodic electrolysis (Figs. 5a and b, Fig. S14 in Supporting information), affirming the superior stability of N-Co_3O_4/NF-2 during HMF oxidation. XPS data show that, after the long-term anodic electrolysis, the ratio of Co^{2+}/Co^{3+} became smaller, and the O1 band decreased meanwhile the O2 band increased (Figs. 5c and d). These results imply the formation of the active species CoOOH during electrolysis [3,41]. The XPS spectrum in N 1s region shows that the intensity of Co-N bond decreases but still remains (Fig. S15 in Supporting information), suggesting the good stability of N-Co_3O_4/NF-2 during anodic electrolysis.

In summary, a controllable nitrogen doping strategy has been demonstrated to significantly improve the catalytic activity of Co_3O_4 nanowires toward the selective oxidation of HMF into FDCA. Through a low temperature treatment in ammonia, N-Co_3O_4/NF samples can be facilely prepared. N dopants can induce the formation of oxygen vacancies and together modulate the electronic structure of Co element and improve the conductivity of Co_3O_4. The resulting defect-engineered N-Co_3O_4/NF-2 exhibits superior HMF oxidation catalytic activity. A HMF conversion rate of 99.5%, a FDCA yield of 96.4% and a Faradaic efficiency of 97.3% can be obtained at a potential of 1.423 V *vs.* RHE. N-Co_3O_4/NF-2 also presents superior catalytic durability and structural stability during HMF oxidation. This work provides a way to develop high-performance electro-catalysts toward HMF conversion through defect engineering.

Declaration of competing interest

The authors declare that they have no known competing financial interests or personal relationships that could have appeared to influence the work reported in this paper.

Acknowledgments

This work was supported by the National Natural Science Foundation of China (Nos. 22075159 and 21775078), and Youth Innovation Team Project of Shandong Provincial Education Department (No. 2019KJC023).

Supplementary materials

Supplementary material associated with this article can be found, in the online version, at doi:10.1016/j.cclet.2021.05.009.

References

[1] D.R. Dodds, R.A. Gross, Chem. Sci. 318 (2007) 1250–1251.
[2] A.J. Ragauskas, C.K. Williams, B.H. Davison, et al., Science 311 (2006) 484–489.
[3] R.A. Sheldon, Green Chem. 16 (2014) 950–963.
[4] K. Gupta, R.K. Rai, S.K Singh, ChemCatChem 10 (2018) 2326–2349.
[5] J.J. Bozell, G.R. Petersen, Green Chem. 12 (2010) 539–554.
[6] K.J. Liu, T.Y. Zeng, J.L. Zeng, et al., Chin. Chem. Lett. 30 (2019) 2304–2308.
[7] S. Rajendran, R. Raghunathan, I. Hevus, et al., Angew. Chem. Int. Ed. 54 (2015) 1159–1163.
[8] M. Sajid, X. Zhao, D. Liu, Green Chem. 20 (2018) 5427–5453.
[9] C. Xu, E. Paone, D. Rodriguez-Padron, R. Luque, F. Mauriello, Chem. Soc. Rev. 49 (2020) 4273–4306.
[10] B. Fang, L. Feng, Acta Phys. Chim. Sin. 36 (2020) 1905020–1905023.
[11] G. Grabowski, J. Lewkowski, R. Skowronski, Electrochim. Acta 36 (1991) 1995.
[12] D.J. Chadderdon, L. Xin, J. Qi, et al., Green Chem. 16 (2014) 3778–3786.
[13] M. Park, M. Gu, B.S. Kim, ACS Nano 14 (2020) 6812–6822.
[14] D.H. Nam, B.J. Taitt, K.S. Choi, ACS Catal. 8 (2018) 1197–1206.
[15] Y. Lu, C.L. Dong, Y.C. Huang, et al., Sci. China Chem. 63 (2020) 980–986.
[16] X. Deng, X. Kang, M. Li, et al., J. Mater. Chem. A 8 (2020) 1138–1146.
[17] H.Y. Sun, G.R. Xu, F.M. Li, et al., J. Energy Chem. 47 (2020) 234–240.
[18] L. Gao, Y. Bao, S. Gan, et al., ChemSusChem 11 (2018) 2547–2553.
[19] N. Zhang, Y. Zou, L. Tao, et al., Angew. Chem. Int. Ed. 58 (2019) 15895–15903.
[20] J. Bai, N. Jia, P. Jin, J. Energy Chem. 51 (2020) 105–112.
[21] X. Huang, J. Song, M. Hua, et al., Green Chem. 22 (2020) 843–849.
[22] S. Barwe, J. Weidner, S. Cychy, et al., Angew. Chem. Int. Ed. 57 (2018) 11460–11464.
[23] B. You, N. Jiang, X. Liu, Y. Sun, Angew. Chem. Int. Ed. 55 (2016) 9913–9917.
[24] N. Jiang, B. You, R. Boonstra, I.M.T. Rodriguez, Y. Sun, ACS Energy Lett. 1 (2016) 386–390.
[25] B. You, X. Liu, N. Jiang, Y. Sun, J. Am. Chem. Soc. 138 (2016) 13639–13646.
[26] Z. Zhou, C. Chen, M. Gao, B. Xia, J. Zhang, Green Chem. 21 (2019) 6699–6706.
[27] E. Hayashi, Y. Yamaguchi, K. Kamata, et al., J. Am. Chem. Soc. 141 (2019) 890–900.
[28] R. Yang, Y. Fan, R. Ye, et al., Adv. Mater. 33 (2021) 2004862.
[29] J. Yang, Z. Zeng, J. Kang, H. Zheng, et al., Nat. Mater. 18 (2019) 970–976.
[30] Z. Wang, H. Liu, R. Ge, et al., ACS Catal. 8 (2018) 2236–2241.
[31] Z. Wang, W. Xu, X. Chen, et al., Adv. Funct. Mater. 29 (2019) 1902875.
[32] J. Sun, W. Xu, C. Lv, et al., Appl. Catal. B Environ. 286 (2021) 119882.
[33] L. Xu, Z. Wang, J. Wang, et al., Nanotechnology 28 (2017) 165402.

[34] J. Zhu, K. Kailasam, A. Fischer, A. Thomas, ACS Catal. 1 (2011) 342–347.
[35] L. Xu, Q. Jiang, Z. Xiao, et al., Angew. Chem. Int. Ed. 55 (2016) 5277–5281.
[36] Z. Xiao, Y.C. Huang, C.L. Dong, et al., J. Am. Chem. Soc. 142 (2020) 12087–12095.
[37] M.J. Kang, H. Park, J. Jegal, et al., Appl. Catal. B. Environ. 242 (2019) 85–91.
[38] M. Cai, Y. Zhang, Y. Zhao, et al., J. Mater. Chem. A 8 (2020) 20386–20392.
[39] P. Kisszekelyi, R. Hardian, H. Vovusha, et al., ChemSusChem 13 (2020) 3127–3136.
[40] Z. Zhang, K. Deng, ACS Catal. 5 (2015) 6529–6544.
[41] B.J. Taitt, D.H. Nam, K.S. Choi, ACS Catal. 9 (2018) 660–670.